J Solid State Electrochem (2012) 16:191–196
DOI 10.1007/s10008-011-1310-2

ORIGINAL PAPER

Linking origin of the electric field-assisted β-PbF_2 crystallization in lead oxyfluoroborate glasses below T_g to simultaneous cathode/anode-compensated electrochemical reactions

José Ezequiel De Souza · Jean-Claude M'Peko

Received: 27 October 2010 / Revised: 10 January 2011 / Accepted: 12 January 2011 / Published online: 2 February 2011

Abstract Full validation of the electrochemical mechanisms so far postulated as driving force of electric field-assisted non-spontaneous crystallization development in given glasses has suffered experimental restrictions. In this work, we looked into origin of this phenomenon in lead oxyfluoroborate glasses, resulting in β-PbF_2 growth even below the corresponding glass transition temperatures, through achieving a systematic study of not only Pt,Ag/Glass/Ag,Pt- but also Pt,Ag/Glass/YSZ:PbF_2/Ag,Pt-type cells, where YSZ:PbF_2 represents a two-phase system (formed by Y_2O_3-doped ZrO_2 and PbF_2). It is demonstrated that crystallization induction in these glasses involves Pb^{2+} ions reduction at the cathode, the phenomenon being, however, confirmed only when the F^- ions were simultaneously also able to reach the anode for oxidation, after assuring either a direct glass–anode contact or percolation pathways for free fluoride migration across the YSZ:PbF_2 mixtures. A further support of this account is that the electrochemically induced β-PbF_2 phase crystallizes showing ramified-like microstructure morphology that arises, accordingly, from development of electroconvective diffusion processes under electric field action.

Keywords Glassy materials · Non-spontaneous crystallization · Electrocrystallization · Electrochemical reactions · Percolation

J. E. De Souza · J.-C. M'Peko (✉)
Grupo Crescimento de Cristais e Materiais Cerâmicos (GCCMC),
Instituto de Física de São Carlos (IFSC),
Universidade de São Paulo (USP),
C. Postal: 369, CEP: 13560-970, São Carlos, São Paulo, Brazil
e-mail: peko@if.sc.usp.br

J.-C. M'Peko
e-mail: jcpeko@yahoo.com

Introduction

Scientific interest on glasses is justified owing to their wide applicability in electrochemical devices such as batteries, fuel cells, sensorial elements, etc. [1, 2]. Nevertheless, application of an electric field and/or atmosphere ambient gradients necessary for executing these applications may alter glassy electrolytes by promoting, for instance, non-spontaneous crystallization phenomena. Examples of this are fresnoite ($Ba_2TiSi_2O_8$) and lithium niobate ($LiNbO_3$) crystalline phases growing, respectively, in $BaO–TiO_2–SiO_2–B_2O_3$ and $Li_2O–Nb_2O_5–SiO_2$ glassy systems when electrically treated well above their respective crystallization temperatures (T_x) [3–6], where no crystallization manifests under usual conditions [1, 2]. The present report refers to a systematic study conducted on lead oxyfluoroborate ($B_2O_3–PbO–PbF_2$) glasses. In literature, development of spontaneous crystallization in fluoride-containing lead borate glasses has been extensively studied [7–9]. By selected heat treatments above the corresponding glass transition temperatures (T_g), lead fluoride (PbF_2)-containing glass ceramics have been produced, with the remark that the crystal system finally synthesized (orthorhombic α-PbF_2 or cubic β-PbF_2) reveals dependent on the initial glass composition and thermal treatment conditions. Interestingly, we have also observed development of electric field-assisted lead fluoride crystallization (β-PbF_2, in this case) in the lead oxyfluoroborate glasses, with the particularity of this phenomenon to manifest even below T_g [10, 11], where crystallization is as well normally unlikely [1, 2]. This hindrance theoretically arises from an increase in rigid glass network-associated viscosity freezing out crystallites nucleation far below T_x.

For development of all the above-mentioned electric field-assisted crystallization phenomena, cation (Ti^{4+}, Nb^{5+}, or Pb^{2+}) reduction at the cathode has been proposed to

exceptionally promote crystallites nucleation, while assuming this reaction to be compensated by anion (O^{2-} or F^-) oxidation at the anode [3–9]. Evidence of, for instance, Ti^{4+} and Pb^{2+} reduction in, respectively, the $BaO–TiO_2–SiO_2–B_2O_3$ and $B_2O_3–PbO–PbF_2$ glassy systems has been provided [4, 10, 11]. Ion reduction is partly expected to induce a decrease of the material viscosity to the point of promoting nuclei formation. Congruently, the above crystallization phenomena have been normally observed to manifest exclusively at the cathode side [3–6, 10, 11]. Conversely, save for assumption, presentation in the literature of a direct evidence of anion oxidation at the anode has been lacking. This is partly justified because detecting molecular O_2(g) or F_2(g) in very few amounts is a relatively hard experimental task, provided that these gases are either easily dissolved or highly reactive in the air ambient.

From the fundamental science (physics and chemistry) viewpoint, nonetheless, postulating the glass–anode interface to be as well active still needs verification to rule or not out any other possible (similar or parallel) mechanism coming into play behind crystallization induction in these glasses when subjected to the electric field action. In fact, occurrence of non-spontaneous glass crystallization in given circumstances has also been proposed to involve, for instance, metal incorporation into glasses, these defects acting subsequently as nuclei formation centers [12–14]. Through the consideration of an original experimental procedure, this work presents a simple but consistent way to explore, in a correlative fashion, the mechanism involved in the induction of these singular, electric field-assisted crystallization phenomena in lead oxyfluoroborate glasses.

Experimental procedure

The present study was conducted on glasses with the $50BO_{1.5}–35PbO–15PbF_2$ composition, hereafter abbreviated as BPP15. The glasses were prepared by applying the melt-quenching technique. That is, well-homogeneized mixtures of oxide reagent grades were melted in a platinum crucible at 780 °C, followed by melt homogenization via stirring for 30 min, the whole preparation process ending with melt quenching to room temperature. Subsequently, the as-produced samples were characterized in terms of differential scanning calorimetry (DSC) (2090 calorimeter, TA), X-ray diffraction (XRD) (Rigaku-Rotaflex RU-200B), and optical microscopy (Leica MZ12.5). As fully justified later in the text, crystallization tests were performed on Pt,Ag/Glass/Ag, Pt- as well as Pt,Ag/Glass/Mixture/Ag,Pt-type cells. The mixture refers to a two-phase ion-conducting medium that was placed at the anode side, and consisting of Y_2O_3-stabilized ZrO_2 plus PbF_2 (YSZ:PbF_2), each component with distinct leading charge carriers: oxygen vacancies [2, 15] and fluoride ions [16, 17], respectively. Ag refers to the electrodes directly fabricated out on the samples, while Pt represents thin plate electrodes from the external set-up. Verification of electric field-assisted development or not of crystallization (under different annealing temperature, time, and electric field strength conditions, see text) included again application of XRD and optical microscopy, plus direct current (DC) (Keithley 610C electrometer) analysis techniques.

Results and discussion

Fig. 1a shows a photographic image of an as-produced BPP15 piece, revealing the originally transparent appearance of the glassy sample. Moreover, Fig. 1b illustrates the DSC curve recorded for a BPP15 sample during its submission to heat treatment over a wide temperature range. From this figure, the values were extracted for, respectively, the glass transition and crystallization temperatures. In the following, Fig. 2 illustrates the XRD patterns from BPP15 samples in different situations. The spectra

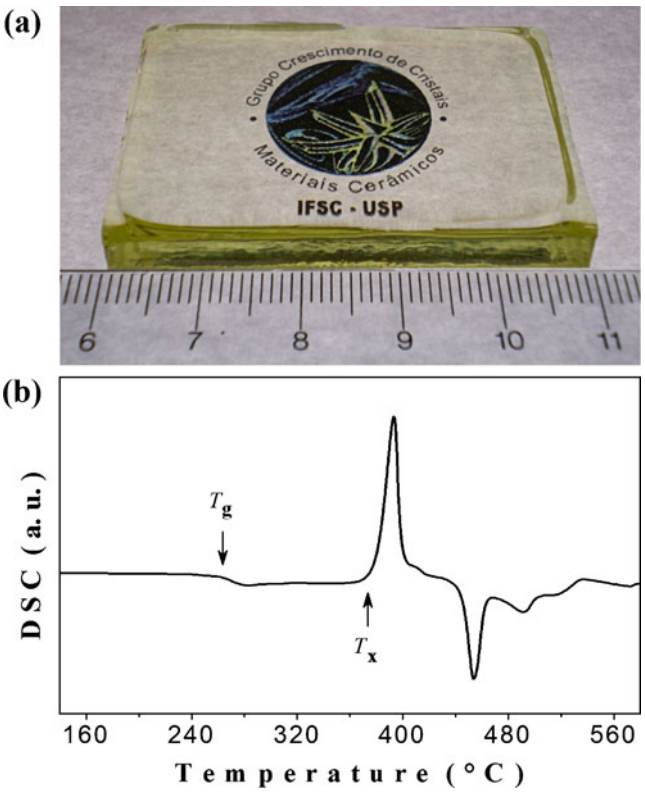

Fig. 1 **a** Photographic image of an as-prepared BPP15 glassy sample after melt quenching. **b** DSC curve registered for a BPP15 sample while rising temperature. Location of the glass transition and crystallization temperatures (T_g≅258 °C and T_x≅380 °C, respectively) is there indicated

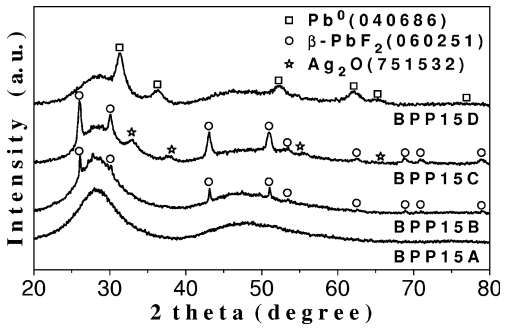

Fig. 2 Room temperature XRD patterns of BPP15 samples studied in this work. *BPP15A*, as-prepared glass; *BPP15B*, sample conventionally treated at 400 °C for 30 min; *BPP15C*, sample treated at 240 °C for 10 h, with $E \cong 0.74$ V/mm; and *BPP15D*, sample treated at 240 °C for 30 h, also with $E \cong 0.74$ V/mm (For BPP15C, Ag_2O formation is attributed to a partial oxidation of the silver electrode in air at high temperature during the long-term electric field-treatment of the sample)

show that the glassy sample (shown in Fig. 1a) is amorphous (BPP15A data), while containing a crystalline phase, identified as β-PbF_2, after glass annealing just above T_x, at 400 °C for 30 min (BPP15B data). The results also evidence β-PbF_2 formation when the sample was treated at 240 °C with a DC electric field of $E \cong 0.74$ V/mm (Pt,Ag/Glass/Ag,Pt-type cell), for 10 h (BPP15C data). In our experiments, crystallization in the BPP15 glasses has been advised with electric fields varying from 3.8–3.6 to 0.7–0.4 V/mm, temperatures ranging from 240 °C to values as low as 150 to 100 °C (hence, even far below T_g), and annealing times varying from 5 to 48 h. In practice, increasing any of these annealing parameters just led to observe, for the BPP15C data in Fig. 2, an increased XRD intensity of the crystallized phase. Figure 3 is an example of optical images from a BPP15 glass sample treated at 150 °C for 48 h, with $E \cong 3.8$ V/mm. The sectional and perspective views (Fig. 3a, b) indicate that crystallization developed at the sample surface that remained in contact with the cathode (negative) electrode, while the sectional and frontal ones (Fig. 3a, c) left no doubt that, important, crystallization exactly occurred only over the sample surface region where this electrode was fabricated out. This means to be dealing here with a kind of surface-controlled crystallization. It is worth pointing out that different from the cases of metal-induced crystallization [12–14], contribution to crystallization from the electrode material must be here discarded, as the phenomenon was always seen to manifest only towards the cathode side (Fig. 3a, b). Further, when annealed below T_g in presence of the Ag electrodes, but under the condition of zero electric field applied, the BPP15 glasses showed no sign of crystallization.

For the above non-spontaneous crystallization phenomenon to happen in BPP15-like glasses, occurrence of the following redox-type electrochemical reactions was rather suggested in previous works [10, 11]: $Pb^{2+}+e^- \rightarrow Pb^+$ at the cathode and $F^- \rightarrow \frac{1}{2} F_2(g)+e^-$ at the anode. Evidence of lead reduction can be in fact advised from the BPP15D data in Fig. 2, revealing formation of metallic Pb^0, together with β-PbF_2 disappearance, for long-term electric field treated samples. This indicates that the whole reaction that gradually occurred at the cathode–glass interface is: $Pb^{2+}+e^- \rightarrow Pb^+$, followed by $Pb^++e^- \rightarrow Pb^0$. For reaction compensation reason, oxidation of the fluoride ions at the anode was opportunely proposed on the basis that these ions really control the electrical transport process in BPP glasses [11, 18–20]. Nevertheless, the remark with respect to all the above refs. [3–6, 10, 11] still is imminence of alternative experimental procedures able to approach sustainability or not of the glass–anode interface activity so far postulated. Regarding the crystallized phase, we just would like to comment that as in the case of the fresnoite ($Ba_2TiSi_2O_8$) containing $BaO–TiO_2–SiO_2–B_2O_3$ glass ceramics, where a low quantity of the reduced titanium

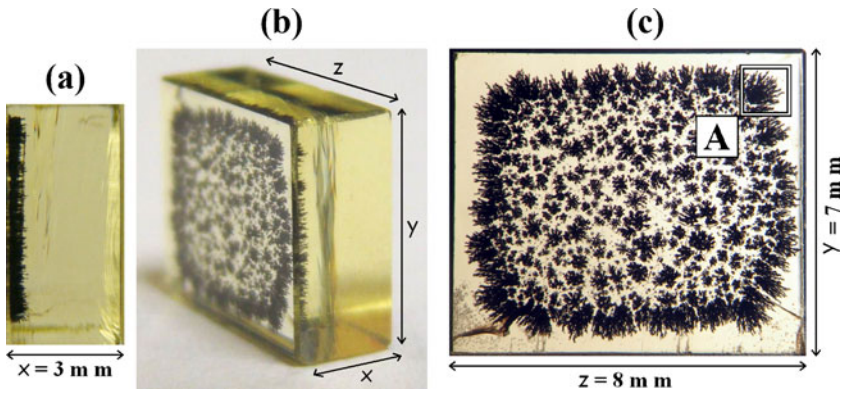

Fig. 3 Photographic images of a BPP15 sample after submission of a Pt,Ag/Glass/Ag,Pt cell to annealing at 150 °C for 48 h, with $E \cong 3.8$ V/mm. **a** Sectional view. **b** Perspective view. **c** Frontal view. Electric field-assisted β-PbF_2 crystallization (with black-like color) developed at the sample surface towards the cathode (negative) electrode. Magnification of the *A* square region indicated in **c** is shown in Fig. 5b for a posterior discussion

ions (Ti^{3+}) incorporates into the fresnoite crystal lattice [8], reduced lead ions (Pb^{+}) should also incorporate into the crystallized lead fluoride (β-PbF_2) phase, which may be then charge-compensated with fluoride ion vacancies, i.e., $PbF_{2-\delta} \equiv Pb_{1-\delta}^{2+}\ Pb_{\delta}^{+}\ F_{2-\delta}^{-}$. Only a continuous reduction reaction of crystal-associated Pb^{+} ions, leading then to metallic lead formation, should account for the simultaneous decomposition of the β-PbF_2 crystalline phase, as detected in Fig. 2 (BPP15D data).

Here, to verify occurrence of the anode activity, if really any, the plan was to study not only conventional Pt,Ag/Glass/Ag,Pt but also Pt,Ag/Glass/YSZ:PbF_2/Ag,Pt cells, allowing discussion of the main subject of concern: how and when do the postulated electrochemical processes (if truly occurring) and crystallization really manifest in terms of nature and/or required conditions? For the second cell configuration, the prepared (100−x)YSZ:$x$$PbF_2$ mixtures were first separately studied in terms of electrical response. Figure 4a presents their DC conductivity (σ) as a function of the PbF_2 volume fraction (V_{PbF_2}), for data collected at 200 °C. Here, $V_{PbF_2} = \left\{1 + \left(m_{(100-x)YSZ}/m_{xPbF_2}\right)F\right\}^{-1} \times 100\%$, where

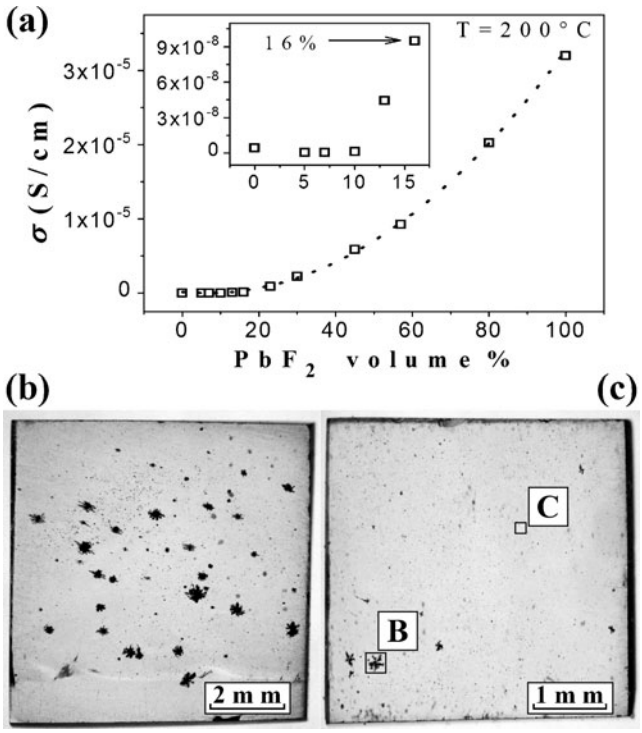

Fig. 4 **a** PbF_2-composition dependence of DC conductivity (σ) measured at 200 °C on the two-phase (100−x)YSZ:$x$$PbF_2$ system. The data show a percolation-like behavior. **b**, **c** Frontal photographic images of BPP15 samples showing β-PbF_2 crystallized regions (with black-like color) after submission of a Pt,Ag/BPP15/70YSZ:30PbF_2/Ag,Pt cell ($V_{PbF_2} = 16\%$) to annealing at 200 and 100 °C, respectively, for 10 h and $E \cong 3.7$ V/mm. Magnifications of the *B* and *C* square regions indicated in **c** are also shown in Fig. 5b for posterior comparison

m_i refers to the mass of each mixture component, while $F = \rho_{PbF_2}/\rho_{YSZ}$ represents the density ratio of just and equally pressed PbF_2 and YSZ powders. Congruent with recognition that normally $\sigma_{PbF_2} >> \sigma_{YSZ}$ (by finally about 3.6 magnitude orders here), the conductivity data in Fig. 4a show a percolation-like behavior, as we intuitively calculated, with a conduction threshold (V_c) locating between 10 and 13 PbF_2 volume percent (Fig. 4a inset). $V_{PbF_2} \equiv V_c$ is the critical volume from which the PbF_2 component would be thus expected to continuously percolate through the YSZ:PbF_2 medium and remains relatively close to the theoretical value of 16% expected for perfectly random 3D systems [21–23]. Of course, assuming validity of the percolation model is here considered just as the dominating conduction mechanism from V_c above, as this model presupposes to be dealing, strictly, with electrical transport through a two-phase system formed by a totally insulating compound and a conducting one, this situation implying that $\sigma \cong 0$ for $V \leq V_c$ and $\sigma = \sigma_o(V - V_c)^s$ for $V \geq V_c$. In Fig. 4a, a value of $s \cong 2.0$ was estimated, still in good agreement with the power-law values of 1.65–2.0 generally referred to as the universal range [21–24].

Hence, while a measurable driving current flowing from the cathode to the anode electrodes can be permanently sustained through the YSZ:PbF_2-containing (Pt,Ag/Glass/YSZ:PbF_2/Ag,Pt-type) cells, the glass crystallization tests can be, however, achieved under different situations of freedom degree for fluoride migration, depending only on the value of the PbF_2 volume fraction (V_{PbF_2}) in the YSZ:PbF_2 mixture placed here at the anode side. For such cells, the situations of $V_{PbF_2} = 0\%, 5\%, 16\%,$ and100% were considered for subsequent study. The main observations extracted from all the experiments that were conducted in this work can be summarized as follows: (1) for the Pt,Ag/Glass/Ag,Pt cell arrangement, β-PbF_2 crystallization was always noted when $E \neq 0$, as was presented above with respect to Fig. 2 (BPP15C data) and Fig. 3; (2) for the Pt,Ag/Glass/YSZ:PbF_2/Ag,Pt case, important, crystallization was prevented when the situations of either $E=0$ or $V_{PbF_2} = 0\%$ and $5\%(V_{PbF_2} < V_c)$ were considered, while turning out to be real when $E \neq 0$ and $V_{PbF_2} = 16\%$ or $100\%(V_{PbF_2} > V_c)$. For illustration, Fig. 4 includes images from BPP15 glasses after submission of a Pt,Ag/BPP15/70YSZ:30PbF_2/Ag,Pt cell ($V_{PbF_2} = 16\%$) to crystallization tests at 200 °C (Fig. 4b) and 100 °C (Fig. 4c) for 10 h, with $E \cong 3.7$ V/mm. Formation of crystalline β-PbF_2 regions was in both cases noted. In brief, while migration of the fluoride ions from the glasses to the anode electrode was frustrated when $V_{PbF_2} < V_c$, the opposite applied when $V_{PbF_2} > V_c$, meaning that these ions were now able to reach this electrode, through the PbF_2 percolation pathways established along the YSZ:PbF_2 mixtures, so as to suffer oxidation.

All these results help to conclusively depict the whole mechanism behind the non-spontaneous crystallization observed in these BPP15 glasses. First, it is clear that neither the electric field nor the electrodes alone had any isolated contribution to development of this phenomenon. Second, besides application of the electric field, the direct contact of not only one but both (cathode and anode) electrodes with the glasses was mandatory to promote β-PbF_2 crystallites nucleation effectively (Pt,Ag/BPP15/Ag, Pt-type cell). This observation also applied when, even in the absence of a direct glass–anode contact, PbF_2 percolation pathways from the glasses to the anode were, however, guaranteed (Pt,Ag/BPP15/$(100-x)$YSZ:$x$$PbF_2$/Ag,Pt-type cell with $V_{PbF_2} > V_c$). Therefore, claiming occurrence in these glasses of the $F^- \rightarrow \frac{1}{2} F_2(g)+e^-$ reaction at the anode absolutely applies, so as compensating the $Pb^{2+}+e^- \rightarrow Pb^+$ reaction that occurs at the cathode and promotes directly crystallites nucleation. In other words, it must be here concluded that origin of the electric field-assisted non-spontaneous crystallization observed in these BPP15 glasses in the glassy state involves a cathode/anode-compensated electrochemical process, totally electrolytic in nature. Notice that the innovative experimental procedure applied in this work, i.e., conduction of crystallization tests in presence of the two-phase YSZ:PbF_2 system that shows either oxygen or fluoride leading charge carriers (depending only on V_{YSZ} or V_{PbF_2} with respect to V_c and, thus, percolation establishment), placed at the anode can be also applied to advance analysis of the conditions (necessary or/and sufficient) under which the electric field-assisted crystallization in, for instance, the above-mentioned $BaO–TiO_2–SiO_2–B_2O_3$ and $Li_2O–Nb_2O_5–SiO_2$ glassy systems occurs.

Another observation that merits to be here commented concerns the distinction between normal and electric field-assisted crystallizations in these glasses in terms of growing β-PbF_2 morphology. In this way, comparison between the images illustrated in Fig. 5 reveals really informative. Figure 5a shows the image of a BPP15 glass sample after annealing at 300 °C (i.e., between T_g and T_x) for 5 h. During thermal treatment, β-PbF_2 regions with a common macro-appearance sprouted spontaneously at the sample surfaces that, compared to the bulk material, are normally expected to act as energetically favored sites for heterogeneous nucleation in glasses [1, 2]. Conversely, for the images shown in Fig. 5b that are magnifications of the A, B, and C square regions indicated in Figs. 3c and 4c (glass samples electrically treated), the crystallized β-PbF_2 phases grew forming, interestingly, ramified-like microstructures. These patterns reproduce well those also found in several other situations of crystallization under electric field action, including electrodeposition of metals from liquid electrolytes [25–28], all classified as resulting from electrolytic phenomena in nature too. Description of origin and evolution of such branched-like patterns has been the subject of some sounding reports [25–29], with the

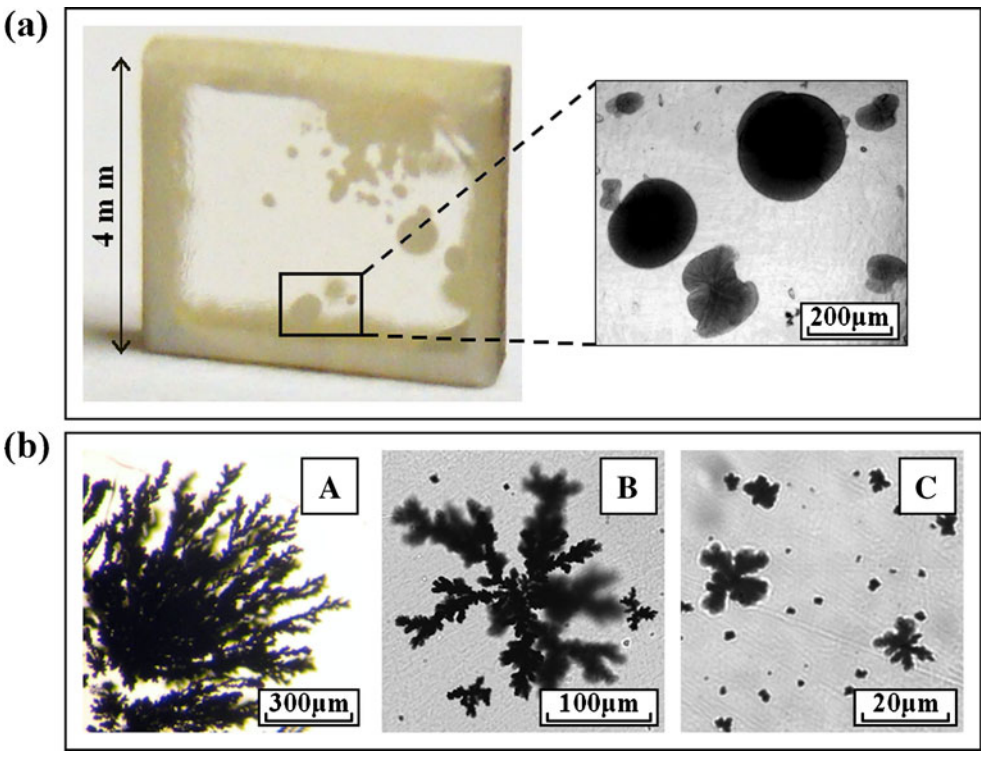

Fig. 5 **a** Photographic image of a BPP15 sample conventionally annealed at 300 °C (between T_g and T_x) for 5 h. The crystallized β-PbF_2 phase shows a common morphology appearance. **b** Magnification of the *A*, *B*, and *C* square regions indicated in Figs. 3c and 4c for the BPP15 glasses electrically treated far below T_g (at 150 °C for 48 h and 100 °C for 10 h, respectively). The crystallized β-PbF_2 phase appears in these cases with ramified-like microstructure morphology

recognition to be in all these cases facing crystallization phenomena under non-equilibrium conditions. At the microscopic level, these unique microstructural events arise from space charges that form at the tips of the nucleated crystallites, so as promoting, under permanent electric field action, electroconvective diffusion processes that lead to the development of ramified-like crystalline phases [26–28]. In the context of this work, what is to be highlighted from the above comparison is that observation of these microstructure patterns in the BPP15 glasses, when electrically treated, is a further proof to be dealing here with a dissimilar, non-conventional crystallization (nucleation and growth) mechanism, involving presently solid-state electrolysis.

Conclusions

In summary, conduction of crystallization tests on not only Pt,Ag/BPP15/Ag,Pt but also Pt,Ag/BPP15/YSZ:PbF_2/Ag,Pt cells has been considered in this work, monitored by XRD and optical microscopy. This study leaves no doubt in rightly establishing that redox-type electrochemical reactions which occur simultaneously at both cathode and anode electrodes, under electric field action, are the driving force responsible for the sub-T_g crystallization observed in lead oxyfluoroborate glasses, resulting in β-PbF_2 electrosynthesis towards the glass–cathode interface. Observation of crystals growing with ramified-like microstructures, which arise from establishment of out-of-equilibrium crystallization conditions that involve, accordingly, electroconvective diffusion processes, is a further support of this concluding statement. The success in fulfilling the present study demonstrates the reliability of the original experimental procedure proposed in this work, remarking that this can be also applied to get insights into real origin or/and mechanism behind development of apparently analogous, electric field-assisted crystallization phenomena in other glassy systems, as those cases cited in this report.

Acknowledgments The authors gratefully acknowledge financial support from the Fundação de Apoio à Pesquisa do Estado de São Paulo (FAPESP) and the Conselho Nacional de Desenvolvimento Científico e Tecnológico (CNPq), two Brazilian research funding agencies.

References

1. Shelby JE (1997) Introduction to glass science and technology. Royal Society of Chemistry, Cambridge
2. Chang Y-M (1997) Physical ceramics. Wiley, New York
3. Gerth K, Rüssel C, Keding R, Schleevoigt P, Dunken H (1999) Phys Chem Glasses 40:135–139
4. Höche T, Kleebe H-J, Brydson R (2001) Phil Mag A 81:825–839
5. Keding R, Rüssel C (1997) J Non-Cryst Solids 219:136–141
6. Keding R, Rüssel C (2005) J Non-Cryst Solids 351:1441–1446
7. Silva MAP, Messadeq Y, Briois V, Poulain M, Ribeiro SJL (2002) J Braz Chem Soc 13:200–206
8. Pisarski WA, Goryczka T, Pisarska J, Ryba-Romanowski W (2007) J Phys Chem B 111:2427–2430
9. Pisarski WA, Goryczka T, Pisarska J, Dominiak-Dzik G, Ryba-Romanowski W (2008) J Non-Cryst Solids 354:492–496
10. De Souza JE, M'Peko J-C, Hernandes AC (2007) Appl Phys Lett 91:064105
11. M'Peko J-C, De Souza JE, Rojas SS, Hernandes AC (2008) J Appl Phys 103:044908
12. Konno TJ, Sinclair R (1995) Phil Mag B 71:163–178
13. Jang J, Oh JY, Kim SK, Choi YJ, Yoon SY, Kim CO (1998) Nature 395:481–483
14. Glebov LB, Glebova L (2002) Glass Sci Technol 75:294–297, Suppl. S
15. M'Peko J-C, De Souza MF (2003) Appl Phys Lett 83:737–739
16. Kennedy JH, Miles R, Hunter J (1973) J Electrochem Soc 120:1441–1446
17. Carr VM, Chadwick AV, Saghafian R (1978) J Phys C Solid State Phys 11:L637–L641
18. Gopalakrishnan R, Tan KL, Chowdari BVR, Vijay AR (1994) J Phys D Appl Phys 27:2612–2618
19. Sokolov IA, Murin IV, Mel'nikova NA, Pronkin AA (2002) Glass Phys Chem 28:296–302
20. Sokolov IA, Murin IV, Mel'nikova NA, Pronkin AA (2002) Glass Phys Chem 28:303–308
21. Zallen R (1983) Chapter 4. The percolation model. In: The Physics of amorphous solids. Wiley, New York
22. McLachlan DS, Blaszkiewicz M, Newnham RE (1990) J Am Ceram Soc 73:2187–2203
23. Landauer R (1978) Electrical conductivity in inhomogeneous media. In: Garland JC, Tanner DB (eds) American Institute of Physics conference proceedings, no.40. Electrical transport and optical properties of inhomogeneous media. American Institute of Physics, New York
24. Kirkpatrick S (1973) Rev Mod Phys 45:574–588
25. Ben-Jacob E, Garik P (1990) Nature 343:523–530
26. Fleury V, Chazalviel J-N, Rosso M (1992) Phys Rev Lett 68:2492–2495
27. Fleury V, Kaufman JH, Hibbert DB (1994) Nature 367:435–438
28. Wang M, Van Enckevort WJP, Ming N-B, Bennema P (1994) Nature 367:438–441
29. Gránásy L, Pusztai T, Börzsönyi T, Warren JA, Douglas JF (2004) Nat Mater 3:645–650